Theoretical Study of CH + O_2 Reactions

Ming-Bao Huang,* Bo-Zhen Chen, and Zhi-Xiang Wang

Graduate School, Academia Sinica, P.O. Box 3908, Beijing 100039, P. R. China

Received: February 12, 2002

DFT B3LYP calculations with the 6-31G(d,p), 6-311G(d,p), 6-311+G(d,p), and 6-311++G(d,p) basis sets were carried out to explore the mechanisms of the CH + $O_2(X^3\Sigma_g^-)$ → CO_2 + H (1) and CH + $O_2(X^3\Sigma_g^-)$ → CO + OH (2) reactions. On the basis of the calculated reaction paths, the two reaction channels are predicted to occur via the following reaction steps. The CH radical initially attacks one of the O atoms of the $O_2(^3\Sigma_g^-)$ molecule, leading to an intermediate HCOO (IM1, $^2A'$), followed by formation of a bond between the C atom and the distal O atom in IM1, leading to an nonplanar structure (intermediate IM2) having a COO ring. The rupture of the O−O bond in IM2 leads to the formyloxyl radical (HCO_2, planar) in its $^2B_2$ state (IM3a). The $^2B_2$ formyloxyl radical (IM3a) can be easily converted into the $^2A_1$ formyloxyl radical (IM3b) via either a transition state ($^2A'$) or crossing of the $^2B_2$ and $^2A_1$ potential energy surfaces. The final products of reaction channels 1 and 2 are obtained from IM3b via trivial chemical processes: (i) for channel 1, an H dissociation process and (ii) for channel 2, H migration from the C center to one of the two O centers leading to an intermediate (OCOH, IM4), followed by cleavage of the central C−O bond in IM4. All these reaction steps have transitions states except the initial step and the step from IM4 to CO + OH. The energies of all the transition states, all the intermediates, the $^2A_1$−$^2B_2$ crossing region, and the final products are lower or much lower than that of the reactants, which indicates that reaction channels 1 and 2 are energetically feasible. The energy levels, structures, and characteristics of the three σ states ($^2A_1$, $^2B_2$, and $^2A'$) of the formyloxyl radical were carefully studied at the B3LYP levels, and the results are compared with previous theoretical results. The initial attack via the least-motion approach (insertion of CH into O_2 directly, leading to IM3b) was examined, but the calculations imply that it is not feasible. The CASSCF and CASPT2 methods were also attempted for the reaction path calculations. It has been noted that quantitatively reliable CAS calculations for these radical reactions would be technically difficult to make at the present stage.

Introduction

The reaction of the methylidyne radical CH($X^2\Pi$) with the oxygen molecule is well-known to be of great importance in combustion chemistry. Work on the CH + O_2 reaction was begun at least 20 years ago,[1] and many experimental studies[1−5] on this reaction have been reported in the literature. Experiment[1] suggests that the reaction has two main channels: one leads to the final products CO_2 + H with a $\Delta H°$ value of −184.0 kcal/mol

$$CH + O_2 \rightarrow CO_2 + H \qquad (1)$$

and the other leads to the final products CO + OH with a $\Delta H°$ value of −159.0 kcal/mol

$$CH + O_2 \rightarrow CO + OH \qquad (2)$$

It is understood that the O_2 molecule as a reactant in reactions 1 and 2 is in its triplet ground state ($X^3\Sigma_g^-$).

The purpose of the present work is to study the mechanisms of reactions 1 and 2 theoretically. To our knowledge, there are very few theoretical papers in the literature that address the CH + O_2 reaction. In 1993, Okada et al.[2] presented some preliminary calculation results on reaction 1 in their experimental paper. In 1987, the HCOO potential energy surface (PES) was partially calculated at the CI level by Schatz et al.[6] from their study on reaction and collisional excitation in H + CO_2, and their paper is somewhat related to the CH + O_2 reaction.

We have devoted our efforts to the theoretical investigation of the CH + O_2 reaction mechanisms and have tried for years to obtain a complete diagram of the CH + O_2 reaction paths by quantum chemical calculations. Recently, we calculated the reaction paths for the two CH + O_2 reactions by using DFT (density functional theory[7,8]) B3LYP (Becke's three-parameter hybrid functional[9] (B3) with the nonlocal correlation of Lee−Yang−Parr[10] (LYP)) method. We have noted that the DFT B3LYP method was used by experimentalists and theoreticians[11] to make successful predictions of the reaction paths (reaction mechanisms) of the C_2H_3 + O_2 reactions. In the present theoretical study, we have predicted the feasible reaction paths from the CH + $O_2(X^3\Sigma_g^-)$ reactants to the final products of reactions 1 and 2 on the basis of B3LYP calculations. We refer to these paths as "the predicted reaction paths" of the CH + O_2 reactions. We also examined other possible (plausible) reaction paths, but they were determined to be unfeasible or represent less important channels by the B3LYP calculations. We refer to these paths as "the examined reaction paths". In addition, we also performed CASSCF[12] (complete active space self-consistent field) reaction path calculations and CASPT2[13,14] single-point energetic calculations for stationary points.

In the present paper, we report the predicted reaction paths (mechanisms) of CH + O_2 reactions 1 and 2 and discuss the results for the examined reaction paths. B3LYP results for the $^2A_1$ and $^2B_2$ states of the formyloxyl radical, as a reaction

* Corresponding author. E-mail: huangmb@es1.gsbustc.ac.cn.

10.1021/jp020424a CCC: $22.00
Published on Web 05/08/2002

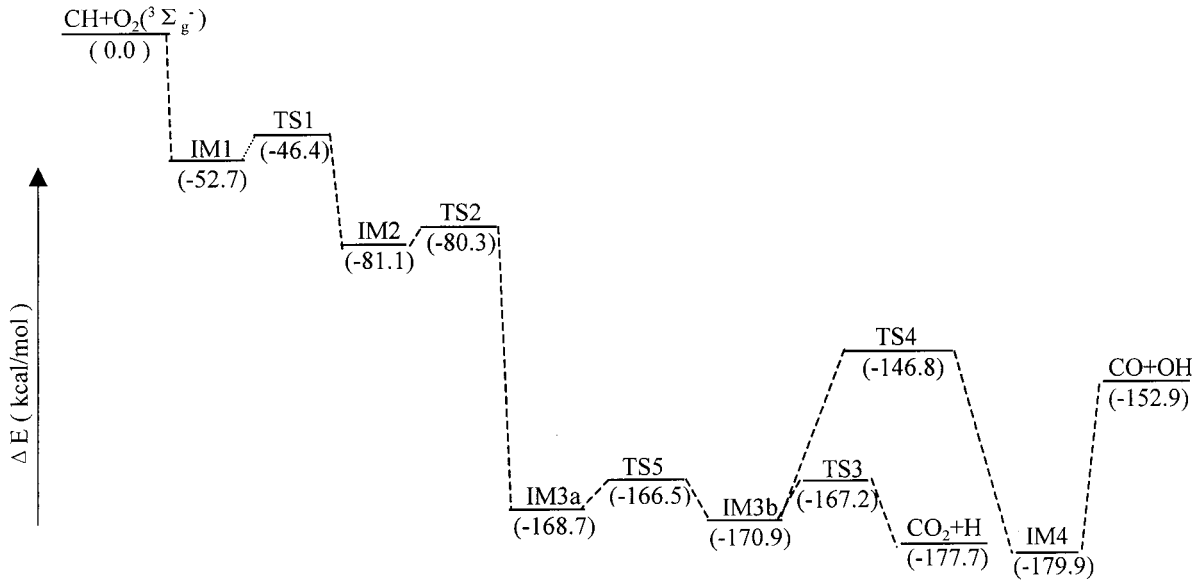

Figure 1. Schematic diagram of the potential energy curves (—) along the predicted reaction paths for the CH + $O_2(X^3\Sigma_g^-) \rightarrow CO_2$ + H and CH + $O_2(X^3\Sigma_g^-) \rightarrow$ CO + OH reactions. The values in parentheses are the B3LYP/6-311++G(d,p) relative energies in kcal/mol (corrected with the B3LYP/6-31G(d,p) zero-point energies).

intermediate, are described in some details. CASSCF and CASPT2 calculation results for the reactions will also be reported and discussed briefly.

Computational Procedure

(U)B3LYP calculations were carried out with the Gaussian 94W suite of programs[15] using 6-31G(d,p), 6-311G(d,p), 6-311+G(d,p), and 6-311++G(d,p) basis sets.[16] The stationary points along the (predicted and examined) reaction paths were scanned in the B3LYP geometry optimization calculations with the four basis sets ("at the four B3LYP levels"). B3LYP/6-31G-(d,p) frequency analysis calculations were performed to characterize stationary points as intermediate complexes (IMs) or transition states (TSs) and to evaluate zero-point energies (ZPEs) that were used to correct the relative energies calculated at the four B3LYP levels. To check the reaction path of each reaction step (see below), we performed B3LYP/6-31G(d,p) (B3LYP/6-311+G(d,p)) IRC (intrinsic reaction coordinate) calculations starting at the transition state and B3LYP/6-31G(d,p) (B3LYP/6-311+G(d,p)) point-wise calculations from reactants to products (or from products to reactants). The point-wise calculations were needed to check the paths of the reaction steps having no transition states (see below). The $\langle S^2 \rangle$ values for all the IMs and TSs along the (U)B3LYP/6-311++G(d,p) reaction paths were less than 0.775.

CASSCF geometry optimization calculations and CASPT2 single-point calculations (incorporating dynamical electron correlation) were performed for the IMs and TSs along the reaction paths using Gaussian 94W and MOLCAS 5.0,[17] respectively.

Predicted Reaction Paths

Figure 1 shows a schematic diagram of the predicted reaction paths for reactions 1 and 2. B3LYP/6-311++G(d,p) energies (corrected with the B3LYP/6-31G(d,p) ZPEs) of IMs, TSs, and the final products relative to that of the CH + $O_2(X^3\Sigma_g^-)$ reactants are given in Figure 1. The optimized structures of IMs and TSs at the four B3LYP levels are given in Figure 2. The relative energies at the four B3LYP levels together with the B3LYP/6-31G(d,p) ZPEs and imaginary frequencies for TSs are listed in Table 1. The relative energies given in Table 1 that were used include the B3LYP/6-31G(d,p) ZPE corrections. We note that the B3LYP/6-311+G(d,p) and B3LYP/6-311++G-(d,p) calculations predict very similar energies and almost identical geometries for each of the IMs and TSs along the predicted reaction paths. The B3LYP/6-311++G(d,p) relative energies and optimized geometries are used unless otherwise noted.

The predicted reaction paths (mechanisms) of CH + $O_2(X^3\Sigma_g^-)$ reactions 1 and 2 in the present study are briefly described as follows (see Figure 1). The CH radical initially attacks one of the O atoms of the $O_2(^3\Sigma_g^-)$ molecule, leading to an intermediate HCOO (IM1, $^2A'$), and this reaction step is strongly exothermic and has no transition state. The initial attack ("side-attack ") step is followed by the formation of a bond between the C atom and the distal O atom in IM1 via a transition state TS1, leading to a nonplanar structure (intermediate IM2) having a C−O−O ring. The ring-opening (the rupture of the O−O bond) in IM2 leads to the formyloxyl radical (HCO_2, planar) in its $^2B_2$ state (IM3a) via a transition state TS2, and this reaction step is strongly exothermic. The $^2B_2$ formyloxyl radical (IM3a) is converted into the $^2A_1$ formyloxyl radical (IM3b) via either a transition state (TS5) or the conical crossing of the $^2B_2$ and $^2A_1$ potential energy surfaces. The final products of reaction channels 1 and 2 are obtained from IM3b via trivial chemical processes: (i) for channel 1, an H dissociation process via a transition state (TS3) and (ii) for channel 2, H migration from the C center to one of the two O centers, leading to an intermediate (OCOH, IM4) via a transition state (TS4), followed by cleavage of the central C−O bond in IM4. The energies of all the transition states, all the intermediates, the crossing point between IM3a and IM3b, and the final products are lower or much lower than that of the reactants, which indicates that reaction channels 1 and 2 are energetically feasible.

In the remainder of this section, we describe the predicted reaction paths step-by-step. However, we must first give a description on the σ electronic states of the formyloxyl radical on the basis of our B3LYP calculations.

***σ* States of the Formyloxyl Radical.** The formyloxyl (HCO_2) radical is characterized by several low-lying electronic states,

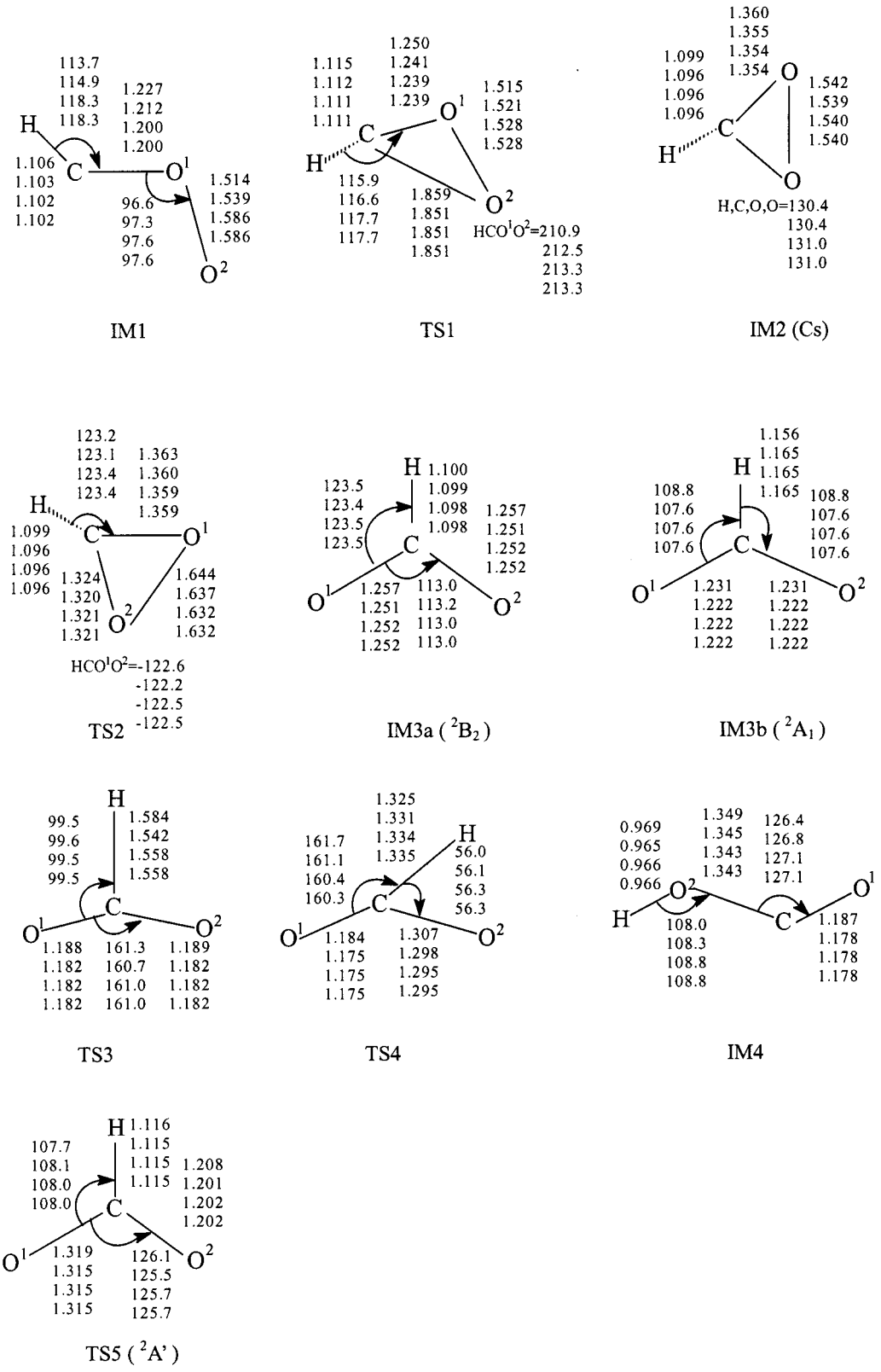

Figure 2. Optimized structures of the intermediate complexes (IMs) and transition states (TSs) along the predicted reaction paths for CH + $O_2(X^3\Sigma_g^-)$ reactions 1 and 2. The values given in the first, second, third, and fourth rows are the parameters optimized at the B3LYP/6-31G(d,p), B3LYP/6-311G(d,p), B3LYP/6-311+G(d,p), and B3LYP/6-311++G(d,p) levels, respectively. Bond lengths are given in Å and angles, in deg. HCO^1O^2 denotes the dihedral angle in TS1 and TS2, and H,C,O,O denotes the angle of the C−H bond out of the OCO plane.

and the three lowest-lying σ states ($^2A_1$, $^2B_2$, and $^2A'$) are involved in the present study. The $^2A_1$ and $^2B_2$ states of the formyloxyl radical were experimentally observed, and the experimental facts[18] indicate that the former state is slightly more stable than the latter. Rauk and co-workers[19,20] studied the energy levels, structures, and characteristics of low-lying (three σ and three π) states of HCO_2 using various ab initio (MP2, MRCI, QCISD, CASSCF, and CASPT2) methods. Some of these states were also studied by Stanton et al.[21] using the EOMIP-CCSD method and by Ayala et al.[22] using nonorthogo-

TABLE 1: Relative Energies[a] of the Intermediate Complexes, Transition States, and Products along the Predicted Reaction Paths for CH + O_2 ($X^3\Sigma_g^-$) Reactions 1 and 2 Calculated at the Four B3LYP Levels (with the Four Basis Sets), Together with the Zero-Point Energies[b](ZPE) and Imaginary Frequencies[b] (IMG) for Transition States

	IMG	ZPE	6-31G(d,p)	6-311G(d,p)	6-311+G(d,p)	6-311++G(d,p)	exptl[c]
CH + $O_2(^3\Sigma_g^-)$		6.4	0.0	0.0	0.0	0.0	
			(−188.80084)[d]	(−188.85676)	(−188.86442)	(−188.86452)	
IM1(^{2}A′)		10.5	−53.1	−52.3	−52.8	−52.7	
TS1	1077i	9.9	−48.5	−46.6	−46.5	−46.4	
IM2		11.9	−85.0	−81.7	−81.1	−81.1	
TS2	2733i	10.7	−83.6	−80.6	−80.3	−80.3	
IM3a($^2B_2$)		12.4	−169.4	−168.8	−168.7	−168.7	
crossing point			(−168.1)[e]	(−167.6)[e]	(−167.6)[e]	(−167.5)[e]	
TS5(^{2}A′)	709i	11.3	−167.1	−166.7	−166.6	−166.5	
IM3b($^2A_1$)		10.2	−170.8	−171.1	−171.0	−170.9	
TS3	986i	7.9	−165.3	−167.8	−167.3	−167.2	
CO_2 + H		7.3	−175.0	−178.9	−177.7	−177.7	−184.0
TS4	1882i	9.1	−145.5	−146.6	−146.8	−146.8	
IM4		13.2	−178.0	−179.6	−180.0	−179.9	
CO + OH		8.4	−146.7	−151.0	−152.9	−152.9	−159.0

[a] Given in kcal/mol and corrected with the B3LYP/6-31G(d,p) ZPEs. [b] Based on the B3LYP/6-31G(d,p) frequency analysis calculations. ZPEs are given in kcal/mol, and imaginary frequencies are given in cm^{-1}. [c] Experimental ΔH^o values from ref 1. [d] Values in parentheses are total energies in au. [e] Relative energies evaluated using total energies (with no ZPE corrections).

TABLE 2: Theoretical Results for the $^2A_1$, ^{2}A′, and $^2B_2$ States of the Formyloxyl Radical Predicted at the Four B3LYP Levels (with the Four Basis Sets) Including Optimized Geometries, Total Energies, and Numbers of Imaginary Frequencies (NImg)[a]

		geometry						
	state	r(H−C)	r(C−O^1)	R(C−O^2)	∠HCO^1	∠HCO^2	total energy	NImg
6-31G(d,p)	$^2A_1$	1.156	1.231		108.8		−189.07919	1[b]
	^{2}A′	1.116	1.319	1.208	107.7	126.2	−189.07506	1
	$^2B_2$	1.100	1.257		123.5		−189.08041	0
6-311G(d,p)	$^2A_1$	1.165	1.222		107.6		−189.13558	1[b]
	^{2}A′	1.115	1.315	1.201	108.1	126.4	−189.13036	1
	$^2B_2$	1.099	1.251		123.4		−189.13529	0
6-311+G(d,p)	$^2A_1$	1.165	1.222		107.6		−189.14306	0
	^{2}A′	1.115	1.315	1.202	108.0	126.3	−189.13781	1
	$^2B_2$	1.098	1.252		123.5		−189.14288	0
6-311++G(d,p)	$^2A_1$	1.165	1.222		107.6		−189.14308	0
	^{2}A′	1.115	1.315	1.202	108.0	126.3	−189.13784	1
	$^2B_2$	1.098	1.252		123.5		−189.14291	0

[a] Bond lengths are given in Å, angles in degrees, and energies in au. [b] The imaginary frequency values are 225i and 52i cm^{-1} at the B3LYP/6-31G(d,p) and B3LYP/6-311G(d,p) levels, respectively.

nal CI and DFT B3LYP(/6-31G(d,p) methods (their B3LYP calculations were performed using a 6-31G(d) basis and only the $^2A_1$ and $^2B_2$ states). Considering the experimental facts, we think that the CASPT2 results of Rauk et al.[19] for the three σ states ($^2A_1$, $^2B_2$, and ^{2}A′) are quite reliable although they performed point-wise calculations for geometry optimization and frequency analyses (their CASSCF results being less reliable or unreliable, see ref 19). Their CASPT2 calculations predict that the $^2A_1$ and $^2B_2$ states represent local energy minima and that the ^{2}A′ state is a transition state. The CASPT2 energetic results indicate that the $^2A_1$ state is the lowest state of the HCO_2 radical and that the $^2B_2$ and ^{2}A′ states are 1.4 and 5.9 kcal/mol higher in energy, respectively, than the $^2A_1$ state. The CASPT2 structure of the $^2A_1$ state has a wide OCO angle of 144.5° and an elongated C−H bond of 1.154 Å, and the $^2B_2$ structure has a considerably smaller OCO angle of 113.0° and a normal-length C−H bond. The CASPT2 structure of the ^{2}A′ state has an OCO angle of 129.8°, and the two C−O bond lengths were 1.323 and 1.205 Å, respectively.

We studied the three σ states ($^2A_1$, $^2B_2$, and ^{2}A′) of the formyloxyl radical by performing B3LYP calculations using the four basis sets, and the total energies, structures, and numbers of the imaginary frequencies for these states that were calculated at the four B3LYP levels are given in Table 2.

At each of the four B3LYP levels, the $^2B_2$ state of the HCO_2 radical is predicted to represent a local minimum and the ^{2}A′ state, to represent a first-order saddle point in the PES. The $^2A_1$ state is predicted to represent a local minimum at the B3LYP/6-311+G(d,p) and B3LYP/6-311++G(d,p) levels. At the B3LYP/6-31G(d,p) and B3LYP/6-311G(d,p) levels, the $^2A_1$ state was predicted to represent a first-order saddle point with small, unique imaginary frequecies (see the footnote for Table 2), and the failure to predict a local-minimum structure was probably caused by the basis sets not being flexible enough. For these reasons, the IRC calculations for the reaction steps with the $^2A_1$ formyloxyl radical (IM3b) as the reactant or product were performed at the B3LYP/6-311+G(d,p) level (see below).

The B3LYP/6-311++G(d,p) results for the $^2A_1$, $^2B_2$, and ^{2}A′ states of the HCO_2 radical are summarized as follows. As mention above, at this level, the $^2A_1$ and $^2B_2$ states are predicted to represent local energy minima and the ^{2}A′ state, a first-order saddle point. The $^2A_1$ state is predicted to be the lowest state of the HCO_2 radical, in agreement with experiment,[18] and the $^2B_2$ and ^{2}A′ states are predicted to be 0.11 and 3.3 kcal/mol higher in energy, respectively, (without ZPE corrections) than the $^2A_1$ state. The $^2A_1$ structure has a wide OCO angle of 144.8° and an elongated C−H bond of 1.165 Å, and the $^2B_2$ structure has a considerably smaller OCO angle of 113.0° and a normal-length

C−H bond. In the unsymmetric $^2A'$ structure, the OCO angle is 125.7°, and the two C−O bond lengths are 1.315 and 1.202 Å, respectively. We note that the present B3LYP/6-311++G-(d,p) calculations and the previous CASPT2 calculations[19] predict the same energy ordering for the three σ states of the HCO_2 radical and very similar structures for each of the states. Also, as shown in Table 2, the B3LYP/6-311+G(d,p) calculations predict almost the same energetic and geometric results for the three states as do the B3LYP/6-311++G(d,p) calculations.

As pointed by many researchers,[19] the different electronic states of the HCO_2 radical are related to different chemical processes. Our B3LYP reaction path calculations for the CH + O_2 reactions indicate that the CH + O_2 reactants are related to the $2B_2$ state (IM3a) of the HCO_2 radical and that the final products of both the reaction channels are related to the $2A_1$ state (IM3b) (see Figure 1). We should describe how the reaction system goes from IM3a($^2B_2$) to IM3b($^2A_1$) (see below), and this has been the bottleneck of the present study. However, before searching feasible paths linking IM3a and IM3b, one should correctly describe (in calculations) the two species themselves, namely, they should be predicted to represent energy minima (intermediates along reaction paths) with the latter slightly more stable than the former.

The previous CASSCF calculations[19] (using the MOLCAS program) for the HCO_2 radical predicted that the $^2A_1$ state represented a first-order saddle point and had higher energy than the $^2B_2$ and $^2A'$ states (both were predicted to represent energy minima by CASSCF calculations), in contrast to the experimental facts.[18] We have found the same problems in our CASSCF calculations for the reaction paths of the CH + O_2 reactions using Gaussian and MOLCAS programs (see below).

From the Reactants to IM3a. The process represented by the portion of the energy profile from the reactants to IM3a (see Figure 1) consists of the first three reaction steps.

The initial reaction step (CH + O_2 → IM1) occurs in the $^2A'$ PES and has no energy barrier (no transition state). The relative energy of IM1 is predicted to be −52.7 kcal/mol, and the initial step is exothermic and can occur easily. To check the reaction path of the initial step, B3LYP/6-31G(d,p) and B3LYP/6-311+G(d,p) point-wise calculations were performed by taking the C−O^1 distance as the reaction coordinate, and the CO^1O^2 angle was found to be larger than 90°, which indicates that the initial step is a side attack by the CH radical on the O_2 molecule.

The relative energies of TS1 and IM2 are predicted to be −46.4 and −81.1 kcal/mol, respectively, the reaction step IM1 → TS1 → IM2 is exothermic by 28.4 kcal/mol, and the barrier energy is evaluated to be 6.3 kcal/mol. Both IM1 and IM2 have C_s symmetry, but the IM1 structure is planar and the IM2 structure is nonplanar (see Figure 2). The structure of TS1 has no symmetry (C_1), and the length of the forming C−O^2 bond (for notation, see Figure 2) is 1.851 Å.

The relative energies of TS2 and IM3a are predicted to be −80.3 and −168.7 kcal/mol, respectively, and the reaction step IM2 → TS2 → IM3a is strongly exothermic (by 87.6 kcal/mol) and has a negligible barrier energy (0.8 kcal/mol). TS2 may disappear in the reaction path calculations of higher levels. The structure of IM3a is C_{2v} symmetric, but the structure of TS2 has no symmetry. The lengths of the breaking O−O bond are 1.540, 1.632, and 2.088 Å in IM2, TS2, and IM3a, respectively.

From IM3a to IM3b. The process of the reaction system from IM3a to IM3b was carefully investigated. We calculated two paths linking IM3a($^2B_2$) and IM3b($^2A_1$) at the B3LYP levels. The reaction system maintains C_s symmetry and is in the $^2A'$ state along one path, and it maintains C_{2v} symmetry along the other path.

Previous CASPT2 calculations predicted the (unique) imaginary frequency in the $^2A'$ state of the HCO_2 radical to be 331i cm^{-1}, and Rauk et al.[19] argued that it was the transition state for the H migration from the carbon atom to the oxygen atom that formed OCOH in the anti conformation, namely, our IM4. Our B3LYP calculations predict the imaginary frequency in the $^2A'$ state to be around 715i cm^{-1}, and normal-mode analysis indicates that it is not the transition state for the H migration process. Our B3LYP/6-311+G(d,p) IRC calculations starting at the $^2A'$ state indicate that the HCO_2 radical goes to a (C_s) structure similar to that (C_{2v}) of IM3a in one direction and to a (C_s) structure similar to that (C_{2v}) of IM3b in the other direction. Therefore, the $^2A'$ structure is considered to be the transition state for a process (a reaction step) from IM3a to IM3b along the $^2A'$ reaction path, and it is denoted as TS5. As shown in Figure 2, the geometry of TS5 is significantly different from that of TS4, which is the proper transition state for the process leading to IM4 (OCOH in the anti conformation, see above). The relative energies of TS5 and IM3b are predicted to be −166.5 and −170.9 kcal/mol, respectively, and the barrier height for the process (IM3a → TS5 → IM3b) occurring on the $^2A'$ PES is evaluated to be only 2.2 kcal/mol.

It has been argued that the $^2B_2$ and $^2A_1$ states of the HCO_2 radical are connected via a conical crossing (intersection) (ref 19 and references therein). However, no detailed descriptions for the crossing of the $^2B_2$ and $^2A_1$ PESs on the basis of theoretical calculations were reported in the literature. In the present work, we have studied the crossing by performing B3LYP/6-311+G(d,p) and B3LYP/6-311++G(d,p) point-wise calculations. For the $^2B_2$ state, the partial geometry optimization calculations were performed at a sequence of fixed OCO angle values in increasing order starting with 113.0°, which is the OCO angle value in the B3LYP/6-311+G(d,p) and B3LYP/6-311++G(d,p) geometries of IM3a, and the energy of the $^2B_2$ state increases monotonically when the OCO angle value increases. For the $^2A_1$ state, the partial geometry optimization calculations were performed at a sequence of fixed OCO angle values in decreasing order starting with 144.8°, which is the OCO angle value in the B3LYP/6-311+G(d,p) and B3LYP/6-311++G(d,p) geometries of IM3b, and the energy of the $^2A_1$ state also increases monotonically when the OCO angle value decreases. These facts imply that the $^2B_2$ and $^2A_1$ PESs should cross each other at an OCO angle value between 113.0° and 144.8°. We located the crossing point (region) at an OCO angle of around 128°, which means that the $^2B_2$ and $^2A_1$ states have very similar energy values and that the $^2B_2$ and $^2A_1$ structures have similar C_{2v} geometries. The energy of the crossing point is 7.2 kcal/mol higher than that of IM3a ($^2B_2$) and 7.3 kcal/mol higher than that of IM3b ($^2A_1$), and these " relative energies " were evaluated using the B3LYP/6-311++G(d,p) total energy values (without ZPE corrections). Though the relative energy of the crossing point is higher than that of TS5, IM3a can also easily convert into IM3b via the $^2B_2$−$^2A_1$ surface crossing.

From IM3b to CO_2 + H. The hydrogen dissociation process (IM3b → TS3 → (CO_2 + H)) occurs on the $^2A_1$ PES. The relative energies of TS3 and CO_2 + H are predicted to be −167.2 and −177.7 kcal/mol, respectively, and the last step of reaction channel 1 is weakly exothermic (by 6.8 kcal/mol) and has a low energy barrier (3.7 kcal/mol). The relative energy value of −177.7 kcal/mol for CO_2 + H is comparable with the experimental $\Delta H°$ value of −184.0 kcal/mol[1] for reaction channel 1. To check the reaction path, B3LYP/6-31G(d,p) and

B3LYP/6-311+G(d,p) point-wise calculations from IM3b to CO_2 + H were performed by taking the C−H distance as the reaction coordinate, and the B3LYP/6-311+G(d,p) IRC calculations were carried out starting at TS3. The leaving species was confirmed to be an H atom (not a proton) on the basis of electronic structure analysis. In the C_{2v} structure of TS3 (see Figure 2), the C−H bond distance is 1.558 Å.

From IM3b to CO + OH. The process represented by the portion of the energy profile from IM3b to CO + OH consists of two reaction steps (see Figure 1), and they occur on the $^2A'$ PES.

The relative energies of TS4 and IM4 are predicted to be −146.8 and −179.9 kcal/mol, respectively, the H migration reaction step (IM3b → TS4 → IM4) is weakly exothermic (by 9.0 kcal/mol), and the barrier energy is evaluated to be 24.1 kcal/mol. The H migration from the C atom to the O^2 atom in IM3b (see Figure 2) leads to IM4 via TS4, and in the structure of IM4, the O^1CO^2H chain is in the trans conformation. To check the reaction path, B3LYP/6-31G(d,p) and B3LYP/6-311+G(d,p) point-wise calculations from IM3b to IM4 were performed by taking the HCO^2 angle (see Figure 2) as the reaction coordinate, and B3LYP/6-311+G(d,p) IRC calculations were carried out starting at TS4. In the migration process, the values of the HCO^2 angle, the H−C distance, and the $H-O^2$ distance of the reaction system vary continuously. The three parameter values are 107.6°, 1.165 Å, and 1.926 Å in IM3b; 56.3°, 1.335 Å, and 1.241 Å in TS4; and 29.0°, 1.890 Å, and 0.966 Å in IM4, respectively. The $C-O^2$ bond lengths in TS4 and IM4 are 1.295 and 1.343 Å, which are significantly longer than the lengths in IM3b.

The last step of reaction channel 2 is a dissociation process (IM4 → (CO^1 + O^2H)). To check the reaction path, point-wise calculations from IM4 to CO + OH were performed by taking the CO^2 distance (see Figure 2) as the reaction coordinate, and no transition state was found. The relative energy of CO + OH is predicted to be −152.9 kcal/mol, and the dissociation step is endothermic by 27.0 kcal/mol. The relative energy value of CO + OH is comparable with the experimental $\Delta H°$ value of −159.0 kcal/mol[1] for reaction channel 2.

After describing the portions of the predicted reaction path from IM3b to the final products of reactions 1 and 2, we will comment on some previous studies reported in the literature. In a 1993 experimental paper, Okada et al.[2] presented their speculation that in the mechanism of reaction 2 the reaction path producing CO + OH might be possible via HCO_2, followed by migration of H. However, their (UHF/4-31G) calculation results for the reaction were very limited and preliminary (they failed to find transition state(s)). In 1987, Schatz et al.[6] calculated part of the HCOO PES at the CI level in their theoretical study of H + CO_2 reactions. Among the species reported in their paper, we found analogues to IMn and TSn along the correct portions of our predicted reaction path to IM3b (see Figure 1). However, their HCO_2 species (characterized as a local minimum at the CI level) had a highly unsymmetric structure that is very similar to that of the $^2A'$ state reported in ref 19 and in the present study.

Examined Reaction Paths

Because the structure of IM3b($^2A_1$) is C_{2v}-symmetric, it is plausible to assume a one-step reaction process from the CH + $O_2(^3\Sigma_g^-)$ reactants to IM3b via the least-motion approach, namely, that the CH radical (with its C atom) attacks the O_2 molecule along one of the perpendicular bisectors of the O−O distance. In the B3LYP/6-311+G(d,p) calculations that we made to examine such an approach, the distance between the C atom and the midpoint (X) of the O−O distance was taken as the reaction coordinate (*Z*). In our single-point B3LYP/6-311+G(d,p) calculations at *Z* values of 3.0, 2.5, 2.0, and 1.6 Å, we failed to force the reaction system to "enter" the proper electronic state of $^2A_1$. B3LYP/6-311+G(d,p) point-wise calculations starting from IM3b were performed on the $^2A_1$ PES, and the reaction system did not approach CH + $O_2(^3\Sigma_g^-)$ when the *Z* value increased. B3LYP/6-311+G(d,p) point-wise calculations starting from IM3b were also performed on the $^2A'$ PES, and it was found that when the *Z* value became larger than 1 Å the CH moiety deviated from the perpendicular bisector of the O−O distance and the O−O distance was considerably elongated. All these testing calculations imply that the assumed one-step insertion reaction, CH + $O_2(^3\Sigma_g^-)$ → IM3b($^2A_1$), via the least-motion approach is not possible. The chemical processes of CH + $O_2(^3\Sigma_g^-)$ reactions 1 and 2 should start with the side attack.

Preliminary CASSCF and CASPT2 Calculations along the Reaction Paths

We tried to describe the reaction paths for the CH + O_2 reactions using the CASSCF method in conjunction with the 6-31G(d,p), 6-311G(d,p), 6-311+G(d,p), and 6-311++G(d,p) basis sets. The CASSCF active space consists of seven electrons and seven orbitals (denoted as CASSCF(7,7)). In our CASSCF geometry optimizations calculations, we located all the IMs and TSs along the B3LYP reaction paths (see Figure 1) except TS2 and TS5. IM1($^2A'$) was located only at the CASSCF(7,7)/6-31G(d,p) level. IM3b($^2A_1$) was predicted to be a local energy minima at the CASSCF(7,7)/6-31G(d,p) level but to be a transition state having large imaginary frequencies (around 2800i cm^{-1}) at the CASSCF(7,7)/6-311G(d,p), CASSCF(7,7)/6-311+G(d,p), and CASSCF(7,7)/6-311++G(d,p) levels. In the remainder of this section, we describe and discuss the results predicted by the CASSCF(7,7)/6-31G(d,p) geometry optimization calculations and CASPT2/6-31G(d,p) single-point energetic calculations at the CASSCF(7,7)/6-31G(d,p) geometries.

The relative energies (including ZPE corrections) of the IMs and TSs and products at both the CASSCF(7,7)/6-31G(d,p) and CASPT2/6-31G(d,p) (CASPT2//CASSCF) levels together with the coefficients for the leading configurations in their CASSCF wave functions are listed in Table 3.

The CASSCF and CASPT2 relative energy values for each of the calculated IMs and TSs are considerably different. For all the calculated stationary-point species, the discrepancies between the CASSCF and B3LYP (/6-31G(d,p)) relative energy values (the B3LYP calculations with the four different basis sets predict very similar relative energy values for each of the species, see Table 1) are large (between 4 and 26 kcal/mol), and the discrepancies between the CASPT2 and B3LYP values are even larger (between 17 and 45 kcal/mol). We note that the absolute values of the CASPT2 relative energies are all smaller than the absolute values of the B3LYP relative energies. The CASPT2 (//CASSCF/6-31G(d,p)) calculations predict that IM3a($^2B_2$) is more stable than IM3b($^2A_1$), which is different from the experimental facts[18] and the prediction based on the B3LYP calculations (see above). The CASPT2 relative energy value of −152.3 kcal/mol for CO_2 + H is much smaller in magnitude than the B3LYP/6-31G(d,p) value of −175.0 kcal/mol and the experimental $\Delta H°$ value of −184.0 kcal/mol.[1] The CASPT2 relative energy value of −129.9 kcal/mol for CO + OH is also much smaller in magnitude than the B3LYP/6-31G(d,p) value of −146.7 kcal/mol and the experimental value of −159.0 kcal/mol.[1]

TABLE 3: Relative Energies[a] (ΔE) of the Intermediate Complexes, Transition States, and Products along the (B3LYP) Reaction Paths for CH + O_2 ($X^3\Sigma_g^-$) Reactions 1 and 2 Calculated at the CASSCF/6-31G(d,p) and CASPT2/6-31G(d,p) Levels, Together with the Coefficients for the Leading Configurations in the CASSCF Wave Functions

ΔE	CASSCF	CASPT2	ΔE	CASSCF	CASPT2
CH + O_2	0.0[c]	0.0	TS5		
IM1	−79.8	−8.0	IM3b($^2A_1$)	−152.6	−133.3
	(0.964)[b]			(0.954)	
TS1	−59.4	−19.6	TS3	−157.1	−137.2
	(0.935)			(0.969)	
IM2	−89.5	−57.0	CO_2 + H	−192.2[c]	−152.3
	(0.957)		TS4	−137.0	−116.3
TS2				(0.975)	
IM3a($^2B_2$)	−161.6	−136.4	IM4	−203.7	−143.1
	(0.966)			(0.974)	
			CO + OH	−165.1[c]	−129.9

[a] Given in kcal/mol and corrected with the CASSCF(7,7)/6-31G(d,p) ZPEs. [b] Values in parentheses are the coefficients for the leading configurations of the CASSCF wave functions. [c] The reactant and product groups (CH + O_2, CO + OH, and CO_2 + H) were treated as three united systems with the distances between the subsystems fixed at separations ≥3.0 Å.

The geometric parameter values in most of the IM and TS structures obtained in the CASSCF optimized calculations (with the four basis sets) are quite different from the B3LYP values. For example, the CASSCF(/6-31G(d,p)) optimized value of 1.347 Å for the C−H bond length in TS3 is 0.237 Å smaller than the B3LYP/6-31G(d,p) value, and the CASSCF value of 100° for the HCO[1] angle in IM1 is 14° smaller than the B3LYP/6-31G(d,p) value. The CASSCF/6-31G(d,p) calculations predict that the crossing between the $^2A_1$(IM3b) and $^2B_2$(IM3a) PESs occurs at ∠OCO = 130°, whereas the B3LYP calculations predict that the crossing occurs at ∠OCO = 128°.

As shown above, the results of our preliminary CASSCF and CASPT2//CASSCF calculations for the reaction paths of the CH + O_2 reactions are not satisfactory. Reliable results for these radical reactions may be obtained in the CASPT2 path calculations with the full-valence active space. The CASPT2 path calculations involve geometry optimization, whereas automatic geometry optimization at the CASPT2 level is not possible at the present stage. Because the structures of the IMs and TSs along the paths have different symmetries (C_s (planar), C_1, C_s (nonplanar), and C_{2v}), it is difficult to find correlations between the molecular orbitals in the electronic structures of all the IMs and TSs. The full-valence active space (17, 13) should be a good choice for the uniform active space in the path calculations. However, such an active space is somewhat too large.

We have checked the coefficients (see Table 3) of the dominant configurations in the CASSCF wave functions of the IMs and TSs, and we realize that the static electron correlation might be somewhat important only for TS1.

Summary

The B3LYP calculations with four basis sets were carried out to explore the mechanisms of the CH + O_2 → CO_2 + H (1) and CH + O_2 → CO + OH (2) reactions. The two reaction channels are predicted to occur via the following reaction steps. The CH radical initially attacks one of the O atoms of the O_2 molecule, leading to IM1($^2A'$), followed by formation of a bond between the C atom and the distal O atom in IM1, leading to a nonplanar intermediate IM2 having a C−O−O ring. The ring-opening in IM2 leads to the formyloxyl radical (HCO_2) in its $^2B_2$ state (IM3a). IM3a can be easily converted into IM3b (the $^2A_1$ formyloxyl radical) via either transition state TS5($^2A'$) or the $^2B_2$−$^2A_1$ PES crossing. The final products of the two channels are obtained from IM3b via trivial chemical processes: (i) for channel 1, an H dissociation process and (ii) for channel 2, H migration from the carbon atom to the oxygen atom to form IM4, followed by cleavage of the central C−O bond in IM4. TS1, IM2, and TS2 have nonplanar structures, whereas the structures of all the other intermediates and transition states along the predicted reaction paths are planar. The energetic results indicate that reaction channels 1 and 2 are energetically feasible. Our testing calculations imply that the plausible one-step least-motion insertion reaction, CH + O_2($^3\Sigma_g^-$) → IM3b($^2A_1$), is not possible. The chemical processes of CH + O_2 reactions 1 and 2 should start with the side attack. We also carried out CASSCF and CASPT2//CASSCF calculations for the reaction paths. It has been noted that quantitatively reliable CAS calculations for these radical reactions are technically difficult at the present stage.

The $^2A_1$, $^2B_2$, and $^2A'$ states of the formyloxyl radical were carefully studied by performing DFT B3LYP calculations. At the B3LYP/6-311+G(d,p) and B3LYP/6-311++G(d,p) levels, the $^2A_1$ and $^2B_2$ states represent local energy minima, and the $^2A_1$ state is predicted to be lower in energy than the $^2B_2$ state, in agreement with experiment.[18] The $^2A'$ state is predicted to be higher in energy than $^2A_1$ and $^2B_2$ and represents a first-order saddle point. On the basis of the B3LYP IRC calculations, the $^2A'$ structure is considered to be the transition state for a process (reaction step) from IM3a($^2B_2$) to IM3b($^2A_1$). The crossing of the $^2B_2$ and $^2A_1$ PESs was studied by performing B3LYP calculations.

Acknowledgment. We appreciate the financial support of this work that was provided by the China National Natural Science Foundation under contracts 29892162 and 20173056.

References and Notes

(1) Lin, M. C. *J. Chem. Phys*. **1974**, *61*, 1835.
(2) Okada, S.; Yamasaki, K.; Matsui, H.; Saito, K.; Okada, K. *Bull. Chem. Soc. Jpn.* **1993**, *66*, 1004.
(3) Bocherel, P.; Herbert, L. B.; Rowe, B. R.; Sims, I. R.; Smith, I. W. M.; Travers, D. *J. Phys. Chem.* **1996**, *100*, 3063.
(4) Taatjes, C. A. *J. Phys. Chem.* **1996**, *100*, 17840.
(5) Markus, M. W.; Roth, P. *Int. J. Chem. Kinet.* **1996**, *28*, 171.
(6) Schatz, G. C.; Fitzcharles, M. S.; Harding, L. B. *Faraday Discuss. Chem. Soc.* **1987**, *84*, 359.
(7) Hohenberg, P.; Kohn, W. *Phys. Rev. B: Condens. Matter* **1964**, *136*, 864.
(8) Kohn, W.; Sham, L. J. *Phys. Rev. A: At., Mol., Opt. Phys.* **1965**, *140*, 1133.
(9) Becke, A. D. *J. Chem. Phys.* **1993**, *98*, 5648.
(10) Lee, C.; Yang, W.; Parr, R. G. *Phys. Rev. B: Condens. Matter* **1988**, *37*, 785.
(11) Mebel, A. M.; Lin, M. C.; Morokuma, K. *J. Am. Chem. Soc*. **1996**, *118*, 9759. (C_2H_3 + O_2).
(12) Roos, B. O. *Adv. Chem. Phys.* **1987**, *69*, 399.
(13) Andersson, K.; Roos, B. O. *Int. J. Quantum Chem.* **1993**, *45*, 591.
(14) Andersson, K.; Malmqvist, P.; Roos, B. O. *Modern Electronic Structure Theory*; Yarkony, D. R., Ed.; World Scientific: Singapore, 1995; Part 1, p 55.
(15) Frisch, M. J.; Trucks, G. W.; Schlegel, H. B.; Gill, P. M. W.; Johnson, B. G.; Robb, M. A.; Cheeseman, J. R.; Keith, T.; Petersson, G. A.; Montgomery, J. A.; Raghavachari, K.; Al-Laham, M. A.; Zakrzewski, V. G.; Ortiz, J. V.; Foresman, J. B.; Cioslowski, J.; Stefanov, B. B.; Nanayakkara, A.; Challacombe, M.; Peng, C. Y.; Ayala, P. Y.; Chen, W.; Wong, M. W.; Andres, J. L.; Replogle, E. S.; Gomperts, R.; Martin, R. L.; Fox, D. J.; Binkley, J. S.; Defrees, D. J.; Baker, J.; Stewart, J. P.; Head-Gordon, M.; Gonzalez, C.; Pople, J. A. *Gaussian 94*; Gaussian, Inc.: Pittsburgh, PA, 1995.
(16) Hehre, W. J.; Radom, L.; Schleyer, P. v. R.; Pople, J. A. *Ab Initio Molecular Orbital Theory;* Wiley: New York, 1986.
(17) Andersson, K.; Blomberg, M. R. A.; Fischer, M. P.; Karlstrom, G.; Lindh, R.; Malmqvist, P.; Neogrady, P.; Olsen, J.; Roos, B. O.; Sadlej, A. J.; Schutz, M.; Seijo, L.; Serrano-Andres, L.; Siegbahn, P. E. M.; Widmark, P.-O. *MOLCAS*, version 5.0; Lund University: Lund, Sweden, 2000.

(18) Kim, E. H.; Bradforth, S. E.; Arnold, D. W.; Metz, R. B.; Neumark, D. M. *J. Chem. Phys.* **1995**, *103*, 7801.
(19) Rauk, A.; Yu, D.; Borowski, P.; Roos, B. *Chem. Phys*. **1995**, *197*, 73 and references therein.
(20) Rauk, A.; Yu, D.; Armstrong, D. A. *J. Am. Chem. Soc.* **1994**, *116*, 8222.
(21) Stanton, J. F.; Kadagathur, N. S. *J. Mol. Struct.* **1996**, *376*, 469.
(22) Ayala, P. Y.; Schlegel, H. B. *J. Chem. Phys.* **1998**, *108*, 7560.